analytical chemistry

Article

Cite This: Anal. Chem. 2019, 91, 10648−10656

pubs.acs.org/ac

Fluorescent Graphitic Carbon Nitride-Based Nanozymes with Peroxidase-Like Activities for Ratiometric Biosensing

Xiaoyu Wang,[†] Li Qin,[†] Minjie Lin,[‡] Hang Xing,[‡] and Hui Wei*[,†,§,∥]

[†]Department of Biomedical Engineering, College of Engineering and Applied Sciences, Nanjing National Laboratory of Microstructures, Jiangsu Key Laboratory of Artificial Functional Materials, Nanjing University, Nanjing, Jiangsu 210093, China

[‡]Institute of Chemical Biology and Nanomedicine, State Key Laboratory for Chemo/Bio Sensing and Chemometrics, College of Chemistry and Chemical Engineering, Hunan University, Changsha, Hunan 410082, China

[§]State Key Laboratory of Analytical Chemistry for Life Science and State Key Laboratory of Coordination Chemistry, School of Chemistry and Chemical Engineering, Nanjing University, Nanjing, Jiangsu 210023, China

[∥]Key Laboratory of Analytical Chemistry for Biology and Medicine (Wuhan University), Ministry of Education, Wuhan 430072, China

Supporting Information

ABSTRACT: While breakthroughs in peroxidase-like nanozymes for bioanalysis have been made, most of current nanozyme biosensing systems are based on a single signal output. Such sensing systems could be easily influenced by environmental and personal factors. We envision that nanozyme sensing systems with ratiometric signal outputs would provide more reliable and robust sensing performance. Herein, to construct such ratiometric sensing systems, three fluorescent graphitic carbon nitride (C_3N_4)-based nanozymes (i.e., C_3N_4−Ru, C_3N_4−Cu, and C_3N_4−hemin) with excellent peroxidase-like activities were prepared. These fluorescent nanozymes emitted a fluorescence at 438 nm when excited at 385 nm. Interestingly, when *o*-phenylenediamine (OPD) was catalytically oxidized to oxidized OPD (OPDox) in the presence of H_2O_2 and nanozymes, the OPDox not only emitted an emerging fluorescence at 564 nm but also quenched the fluorescence at 438 nm of the nanozymes. We therefore employed the ratio of the fluorescent intensity at 564 and 438 nm (i.e., F_{564}/F_{438}) as the signal output to construct the ratiometric biosensing systems. First, we used the C_3N_4−Ru nanozyme to construct the ratiometric H_2O_2 sensing system, which showed not only the enhanced robustness but also wider linear range and better sensitivity than most reported H_2O_2 sensors based on nanozymes. Second, with the assistance of glucose oxidase, glucose can be detected by such ratiometric sensing systems. Third, we used three different C_3N_4-based nanozymes to construct ratiometric sensor arrays for the detection and discrimination of five phosphates. This study provides new insights for constructing robust nanozyme biosensing systems.

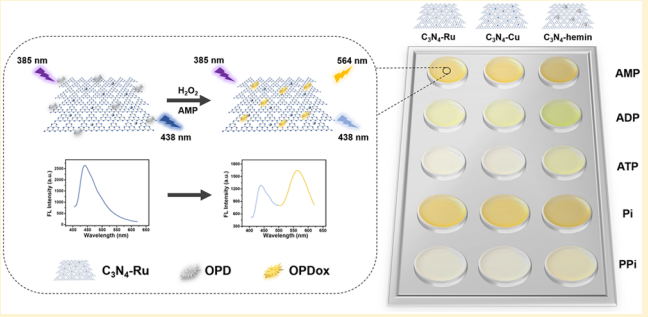

Nanozymes are functional nanomaterials with enzyme-like characteristics, which are superior to natural enzymes as well as conventional molecular and polymeric enzyme mimics.[1−5] Because of their tunable catalytic activities and multiple functionalities, nanozymes have been applied to many fields, ranging from biosensing and biomedical imaging to therapeutics and environmental protection.[6−24] Among them, peroxidase-mimicking nanozymes have been extensively studied to construct biosensors for versatile analytes including nucleic acids, metal ions, bioactive small molecules, biomacromolecules, etc.[25−43] For example, H_2O_2 detection was conducted by monitoring the signal change of a peroxidase substrate, which was oxidized by H_2O_2 in the presence of peroxidase-mimicking nanozymes.[7,30,32,34,37] In addition, some analytes could be oxidized by their corresponding oxidases to produce H_2O_2.[7,30,32,34,37] Therefore, these targets (e.g., glucose, lactate, and sarcosine) can be detected by combining their corresponding oxidases with peroxidase-like nanozymes.[7,30,32,34,37] Immunoassays for protein detection were also developed using peroxidase-mimicking nanozymes as tags for signaling.[2,8,17,44] Recently, colorimetric sensor arrays were constructed using nanozymes with peroxidase-like activities for detection and discrimination of small molecules, proteins, and cells.[39,45−47] Despite these substantial successes, most of the current nanozyme-based biosensors and sensor arrays were constructed using a single colorimetric or fluorescent sensing signal, which could be easily influenced by environmental and personal factors. We envision that a nanozyme biosensor with a

Received: April 18, 2019
Accepted: July 18, 2019
Published: July 18, 2019

DOI: 10.1021/acs.analchem.9b01884
Anal. Chem. 2019, 91, 10648−10656

ratiometric signal output would provide more reliable and robust diagnostics.[48−51]

Graphitic carbon nitride (i.e., C_3N_4) nanosheets, one type of graphene-like two-dimensional nanomaterials with unique electronic structure and optical properties, have exhibited broad applications in sustainable energy, biosensing, etc.[40,52−54] For example, C_3N_4 and horseradish peroxidase were used for constructing a ratiometric fluorescence sensing platform, enabling robust detection of H_2O_2 and glucose.[54] Recent studies reported that C_3N_4 nanosheets could act as peroxidase mimics for colorimetric detection of H_2O_2, glucose, and exosomes.[40,55] However, the peroxidase-like activity of C_3N_4 nanosheets was far from satisfactory, which limited their further applications. The abundant pyridinic nitrogen moieties and π-conjugated framework in C_3N_4 nanosheets provide potential binding sites for further modifications to enhance the catalytic activity of the pristine C_3N_4 nanozymes. Herein, we reported three different fluorescent C_3N_4-based nanozymes (i.e., C_3N_4−Ru, C_3N_4−Cu, and C_3N_4−hemin) with excellent peroxidase-like activities. Ruthenium or copper ions could be embedded into nanosheets through the coordination of metal ions with pyridinic nitrogen moieties of C_3N_4, while hemin could be bound to C_3N_4 through the π−π interaction. These C_3N_4-based nanozymes with peroxidase-like activities and fluorescence emission at 438 nm were termed as fluorescent nanozymes.

On the basis of these fluorescent nanozymes, ratiometric fluorescent sensing methods were developed. These C_3N_4-based nanozymes exhibited fluorescence peaks at 438 nm upon excitation at 385 nm. In the presence of H_2O_2 and *o*-phenylenediamine (OPD), C_3N_4-based nanozymes can catalyze the oxidation of OPD to form OPDox, which not only emitted fluorescence at 564 nm but also significantly quenched the fluorescence at 438 nm of C_3N_4-based nanozymes. The fluorescence intensity ratio (F_{564}/F_{438}) increased with the increase of the concentration of H_2O_2, which enabled the development of a ratiometric fluorescent method for bioanalysis. To demonstrate the robustness of the fluorescent nanozyme-based ratiometric sensing method, two applications were demonstrated in this work. We first used C_3N_4−Ru as a fluorescent peroxidase mimic for ratiometric detection of H_2O_2 and the H_2O_2-generating biomolecule (i.e., glucose). Moreover, we used C_3N_4−Ru, C_3N_4−Cu, and C_3N_4−hemin to fabricate ratiometric fluorescent sensor arrays for phosphates detection and discrimination. Phosphates play critical roles in cellular signaling and energy metabolism in biological systems.[56] The peroxidase-like activities of C_3N_4-based nanozymes could be tuned by phosphates, which formed the basis of the ratiometric fluorescent sensor arrays for phosphates discrimination. Five phosphates including adenosine 5′-triphosphate disodium salt (ATP), adenosine 5′-diphosphate sodium salt (ADP), adenosine 5′-monophosphate sodium (AMP), pyrophosphate (PPi), and phosphate (Pi) were successfully discriminated not only in aqueous solutions but also in serum samples. Additionally, the usefulness of the ratiometric array was further demonstrated by detecting unknown blind samples, where 20 unknown samples containing phosphates were accurately identified with 95% accuracy.

EXPERIMENTAL SECTION

Chemicals and Materials. Adenosine 5′-monophosphate sodium (AMP) was obtained from Sigma-Aldrich. Ruthenium chloride hydrate ($RuCl_3{\cdot}xH_2O$), hemin, adenosine 5′-triphosphate disodium salt (ATP), adenosine 5′-diphosphate sodium salt (ADP), 3,3′,5,5′-tetramethylbenzidine dihydrochloride (TMB), 2,2′-azinobis (3-ethyl benzothi-azoline-6-sulfonic acid) ammonium (ABTS), hydrogen peroxide, and glucose oxidase were purchased from Aladdin Chemical Reagent Co., Ltd. Sodium phosphate tribasic dodecahydrate ($Na_3PO_4{\cdot}12H_2O$, Pi), melamine, *o*-phenylenediamine (OPD), and sodium acetate trihydrate were purchased from Sinopharm Chemical Reagent Co., Ltd. Sodium pyrophosphate (PPi) was purchased from Kermel Reagent. Copper chloride dihydrate ($CuCl_2{\cdot}2H_2O$) was obtained from Nanjing Chemical Reagent Co., Ltd. All aqueous solutions used in the experiments were prepared with deionized water (18.2 MΩ·cm, Millipore).

Instrumentation. Transmission electron microscopy (TEM) images were recorded on a JEOL JEM-2100 transmission electron microscope at an acceleration voltage of 200 kV. UV−visible absorption spectra were collected using a spectrophotometer (TU-1900, Beijing Purkinje General Instrument Co. Ltd., China). The absorption of a 96-well plate at 450 nm was recorded by a microplate reader (Infinite M200 PRO, Tecan). X-ray photoelectron spectroscopy (XPS) was collected using a PHI 5000 VersaProbe (Ulvac-Phi, Japan). Fluorescent spectra were obtained on a Hitachi F-4600 fluorescent spectrometer (Japan).

Synthesis of C_3N_4 Nanosheets. The bulk C_3N_4 was synthesized by pyrolysis of melamine.[57] Briefly, melamine (6 g) was placed in a ceramic crucible with a cover and subsequently heated at 600 °C for 2 h with a heating rate of 3 °C/min. To obtain the C_3N_4 nanosheets, 1 g of bulk C_3N_4 powder was dispersed in 100 mL of 5 M HNO_3 and refluxed for 24 h. The product was washed with deionized water for several times until near-neutral pH. Finally, the obtained C_3N_4 suspension was sonicated for 24 h and centrifuged at 6000 rpm for 20 min to remove the unexfoliated nanosheets.

Synthesis of C_3N_4−Ru, C_3N_4−Cu, and C_3N_4−Hemin. To synthesize C_3N_4−Ru, 10 mg of C_3N_4 nanosheets were first dispersed into 10 mL of ultrapure water. Subsequently, 40 μmol of $RuCl_3{\cdot}xH_2O$ was added into the above solution, which was then refluxed for 4 h. The C_3N_4−Ru was obtained by centrifuging and washing with water twice to remove the excess $RuCl_3$.[58] C_3N_4−Cu was prepared in a similar fashion where an equivalent amount of $CuCl_2{\cdot}2H_2O$ precursor was used instead of $RuCl_3{\cdot}xH_2O$.

In a typical synthesis of C_3N_4−hemin, 7.5 mg of C_3N_4 nanosheets, 7.5 mg of hemin, and 150 μL of ammonia (28%) were mixed into 30 mL of ultrapure water. The mixture was stirred at 60 °C for 6 h. The C_3N_4−hemin was obtained by centrifuging and washing with water twice to remove the excess hemin.

Peroxidase-Like Activity Measurements. To determine the peroxidase-like activity of the C_3N_4-based nanozymes, 50 μL of a 100 μg/mL nanozyme solution, 100 μL of 200 mM H_2O_2, and 100 μL of 20 mM OPD were added into 750 μL of 200 mM acetate buffer solution (pH = 4.5). The final concentrations of nanozymes, H_2O_2, and OPD were 5 μg/mL, 20 mM, and 2 mM, respectively. After mixing, the reaction solution was immediately used for UV−visible spectroscopic measurements at 37 °C, and the relative activities of the nanozymes were calculated as follows:

DOI: 10.1021/acs.analchem.9b01884
Anal. Chem. 2019, 91, 10648−10656

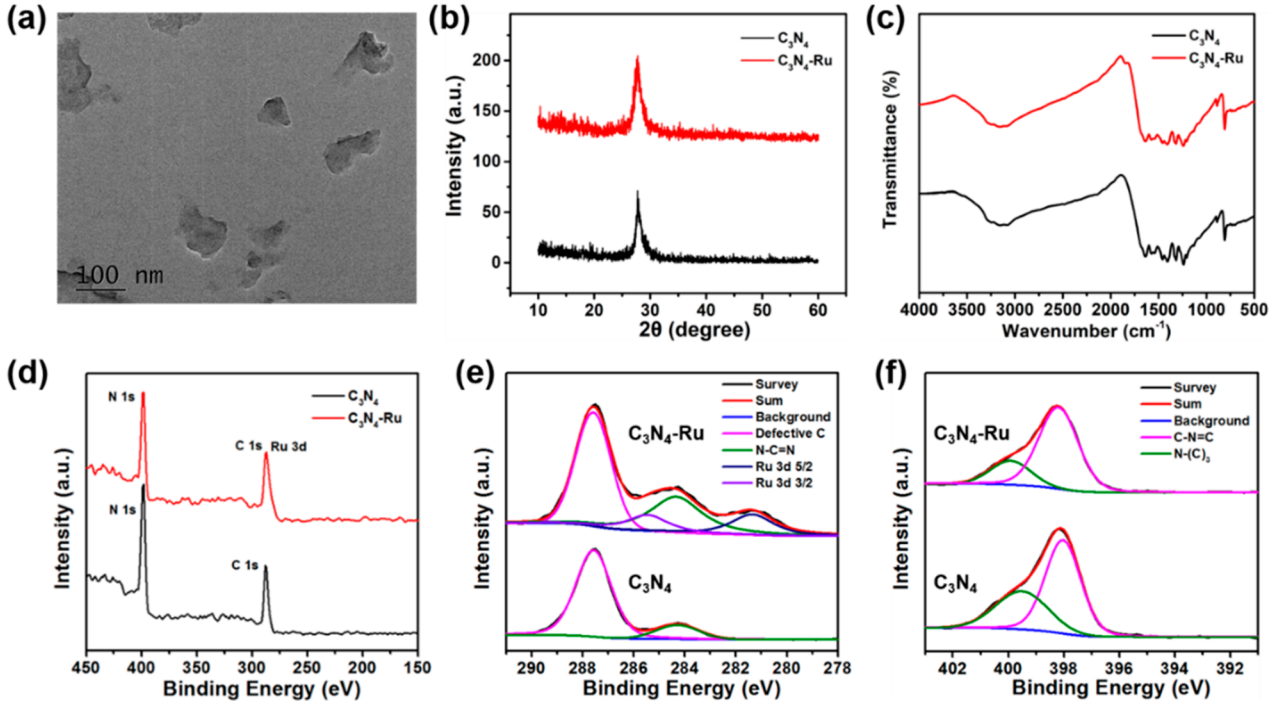

Figure 1. (a) TEM image of as-synthesized C_3N_4−Ru nanosheets. (b) Powder X-ray diffraction patterns and (c) Fourier transform infrared spectra of C_3N_4 and C_3N_4−Ru. (d) Survey X-ray photoelectron spectra (XPS) of C_3N_4 and C_3N_4−Ru. High-resolution XPS spectra of (e) C 1s and Ru 3d and (f) N 1s in C_3N_4 and C_3N_4−Ru.

$$\text{relative activity} = \frac{A_{\text{with nanozyme, 450 nm, 120 second}} - A_{\text{with nanozyme, 450 nm, 0 second}}}{A_{\text{with } C_3N_4\text{, 450 nm, 120 second}} - A_{\text{with } C_3N_4\text{, 450 nm, 0 second}}} \quad (1)$$

Ratiometric Detection of H_2O_2 and Glucose Using C_3N_4−Ru Nanozyme. H_2O_2 detection was carried out as follows: (1) 10 μL of C_3N_4−Ru nanosheets (100 μg/mL), 10 μL of OPD (20 mM), and 70 μL of NaOAc buffer (0.2 M, pH 4.5) were added into each well of a 96-well plate. (2) 10 μL of H_2O_2 with various concentrations was added into the above reaction solution. (3) The mixed solution was incubated for 40 min at 37 °C. Then, the absorbance at 450 nm and fluorescence at 438 and 564 nm of each sample were recorded by a microplate reader.

Glucose detection was carried out as follows: (1) 100 μL of glucose oxidase (0.5 mg/mL) and 100 μL of glucose with different concentrations in 50 mM Tris-HCl buffer (pH 7.4) were incubated for 40 min at 37 °C. (2) 60 μL of NaOAc buffer (0.2 M, pH 4.5), 20 μL of the incubated solution, 10 μL of C_3N_4−Ru nanosheets (100 μg/mL), and 10 μL of OPD (20 mM) were subsequently added into each well of a 96-well plate. (3) The mixed solution was incubated for 40 min at 37 °C. Then, the absorbance at 450 nm and fluorescence at 438 and 564 nm of each sample were recorded by a microplate reader.

Discrimination of Phosphates Using Ratiometric Fluorescent Sensor Arrays. Phosphates were detected as follows: 40 μL of phosphate solution with a certain concentration was mixed with the C_3N_4-based nanozymes and incubated for 10 min. The total volume of the mixed solution was 200 μL. The concentration of C_3N_4-based nanozymes was 100 μg/mL. Then, 10 μL of the incubated solution, 70 μL of NaOAc buffer (0.2 M, pH 4.5), 10 μL of H_2O_2 (10 mM for C_3N_4−Ru, 2 M for C_3N_4−Cu and C_3N_4−hemin), and 10 μL of OPD (20 mM) were subsequently added into each well of a 96-well plate. Immediately after the addition of OPD, the absorbance at 450 nm and fluorescence at 438 and 564 nm of each sample were recorded by a microplate reader at an interval of 10 min for 40 min. Totally, 5 kinds of phosphates were tested against the 3 kinds of C_3N_4-based nanozymes 5 times. Each test produced a training-data matrix of 5 phosphates × 3 arrays × 5 replicates. The data were processed by linear discriminant analysis (LDA).

RESULTS AND DISCUSSION

Synthesis and Characterization of C_3N_4-Based Nanozymes. C_3N_4−Ru and C_3N_4−Cu were prepared by refluxing the mixture of C_3N_4 and $RuCl_3{\cdot}xH_2O$ (or $CuCl_2{\cdot}2H_2O$) in an aqueous solution according to previous methods.[58] The Ru^{3+} or Cu^{2+} can be effectively incorporated into C_3N_4 because the rich pyridinic nitrogen atoms of C_3N_4 provided strong coordination sites for metal ions. The morphologies of the C_3N_4-based nanozymes were investigated by transmission electron microscopy (TEM). As shown in Figures 1a, S1, and S2a, both C_3N_4−Ru and C_3N_4−Cu exhibited very similar sheet structures to C_3N_4 nanosheets, indicating that the synthetic procedures did not affect the morphology of C_3N_4. By powder X-ray diffraction measurements, C_3N_4−Ru, C_3N_4−Cu, and C_3N_4 displayed a single diffraction peak centered at 27.2° (Figures 1b and S2b). The peak was originated from an interplanar spacing of 0.326 nm, which was the characteristic peak of the C_3N_4 (002) plane. No additional diffraction peaks were observed after refluxing the Ru^{3+} or Cu^{2+} with C_3N_4, demonstrating that both C_3N_4−Ru and C_3N_4−Cu retained the same structure with C_3N_4 and no crystalline Ru or Cu was formed. The chemical structures of C_3N_4−Ru and C_3N_4−Cu were investigated by Fourier transform infrared (FT-IR)

DOI: 10.1021/acs.analchem.9b01884
Anal. Chem. 2019, 91, 10648−10656

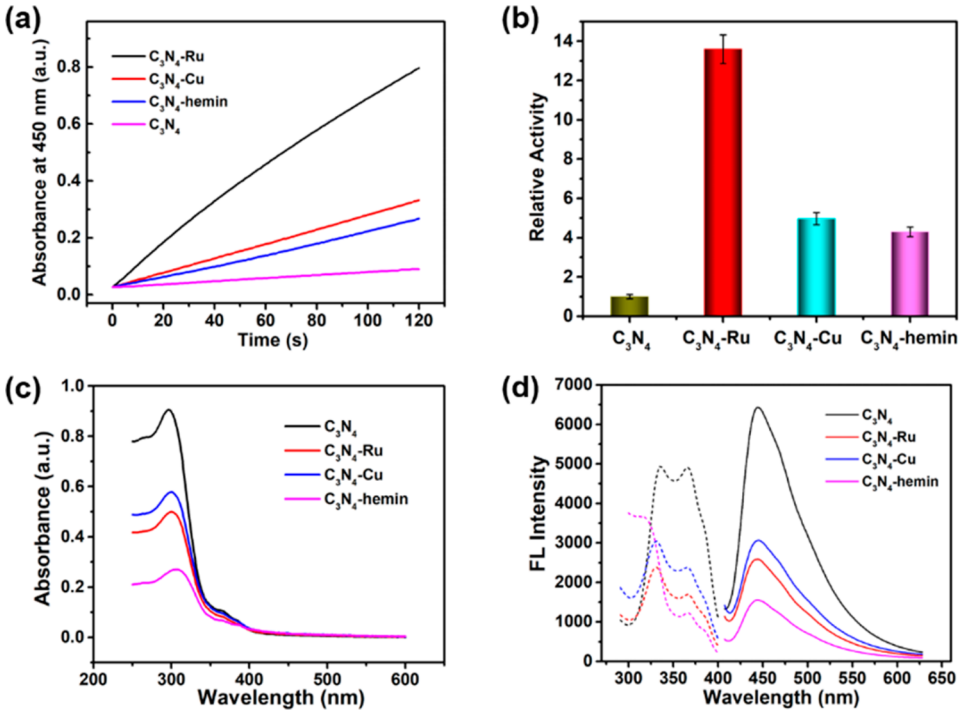

Figure 2. (a) Kinetic curves of A_{450} for monitoring the catalytic reaction of 2 mM OPD with 20 mM H_2O_2 in the presence of 5 μg/mL C_3N_4, C_3N_4−Ru, C_3N_4−Cu, and C_3N_4−hemin. (b) Comparison of the peroxidase-like activities of different C_3N_4-based nanozymes. (c) UV−visible absorption spectra, (d) Fluorescence excitation (dashed lines), and emission spectra (solid lines) of 10 μg/mL C_3N_4, C_3N_4−Ru, C_3N_4−Cu, and C_3N_4−hemin.

spectroscopy. As shown in Figures 1c and S2c, nearly identical characteristic spectra for C_3N_4, C_3N_4−Ru, and C_3N_4−Cu were observed, demonstrating that the coordination of Ru^{3+} or Cu^{2+} did not disturb the structure of C_3N_4. The peak at 810 cm^{-1} originated from the breathing of tris-triazine units, and the bands in the region of 1000−1800 cm^{-1} were attributed to the stretching vibration of aromatic CN heterocycles.

Taking C_3N_4−Ru as an example, we studied the chemical composition and oxidation states of C_3N_4-based nanozymes by X-ray photoelectron spectroscopy (XPS). Figure 1d shows the survey spectra of C_3N_4 and C_3N_4−Ru, where two distinct peaks with binding energy at 284 and 399 eV belonged to C 1s and N 1s, respectively. In addition, two additional peaks at about 282 and 462.5 eV were observed in the C_3N_4−Ru sample, which could be assigned to Ru 3d and Ru 3p, indicating that Ru ions were successfully incorporated into the C_3N_4 skeletons (Figures 1d and S3). The high-resolution spectra of C 1s and Ru 3d are shown in Figure 1e. The high-resolution C 1s spectra of C_3N_4 and C_3N_4−Ru could be deconvolved into two peaks with binding energy at 284.3 and 287.5 eV, respectively. The peak located at 287.5 eV was assigned to the sp^2-hybridized carbon in N—C═N of the C_3N_4 skeleton, while the other peak was assigned to the defective carbon in sp^3 C−C bonds. To identify the oxidation state of Ru in the C_3N_4−Ru, we further analyzed the high-resolution spectrum of Ru 3d. As shown in Figure 1e, the Ru 3d electrons were deconvoluted into two peaks at 281.35 and 285.45 eV, which were ascribed to Ru $3d_{5/2}$ and Ru $3d_{3/2}$, respectively. Moreover, these binding energies of Ru 3d were very similar to those of 3d electrons of Ru^{2+} ions in a ruthenium tris-bipyridine complex, suggesting that Ru^{3+} may be reduced into Ru^{2+} by hydroxide species during refluxing.[58−60] The N 1s spectra of C_3N_4 and C_3N_4−Ru were deconvoluted into two subpeaks (Figure 1f). For C_3N_4, peaks centered at 398.04 and 399.50 eV were observed, which were attributed to sp^2-hybridized pyridinic nitrogen (i.e., C—N═C) and sp^3-hybridized tertiary nitrogen (N−$(C)_3$), respectively. Notably, the binding energy of C—N═C in C_3N_4−Ru was 0.15 eV higher than that of C_3N_4, which can be attributed to the electron transfer from nitrogen atoms in C_3N_4 to Ru ions. The above-mentioned results demonstrated that the Ru ions were successfully incorporated into the C_3N_4 skeleton by Ru−N coordination. The high-resolution Cu 2p spectra of C_3N_4−Cu also demonstrated that Cu ions were successfully coordinated with C_3N_4 (Figure S2d).

The C_3N_4−hemin was prepared by stirring the mixture of C_3N_4 and hemin at 60 °C. The characterization and analysis of C_3N_4−hemin were shown in Figure S4.

Peroxidase-Like Activity and Optical Property. After establishing the successful preparation of C_3N_4-based nanozymes, their peroxidase-like activities were investigated. Among the obtained three C_3N_4-based nanozymes, C_3N_4−Ru exhibited the best catalytic activity (vide infra). Therefore, C_3N_4−Ru was taken as an example to evaluate the intrinsic catalytic activity of C_3N_4-based nanozymes. The peroxidase-like activity of C_3N_4−Ru was first evaluated by catalyzing the oxidation of a typical chromogenic substrate OPD in the presence of H_2O_2. As shown in Figure S5a, C_3N_4−Ru along with H_2O_2 and OPD exhibited a deep yellow color with a strong absorption at 450 nm. In contrast, other control groups showed a negligible color change. Two other typical peroxidase-like substrates (i.e., TMB and ABTS) were used to further demonstrate the peroxidase-like activity of C_3N_4−Ru. As seen in Figure S5b, C_3N_4−Ru also can catalyze the oxidation of TMB and ABTS in the presence of H_2O_2, and blue and green oxidized products with characteristic

DOI: 10.1021/acs.analchem.9b01884
Anal. Chem. 2019, 91, 10648−10656

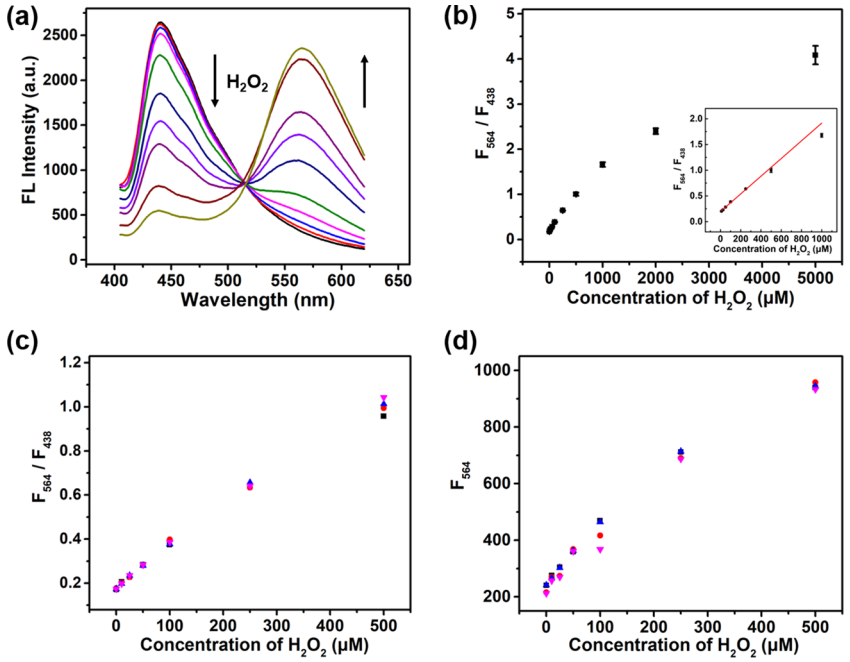

Figure 3. (a) Fluorescence spectra of C_3N_4−Ru nanozyme in the presence of 0, 10, 25, 50, 100, 250, 500, 1000, 2000, and 5000 μM of H_2O_2. (b) Fluorescence intensity ratio (F_{564}/F_{438}) as a function of H_2O_2 concentration. Inset: linear calibration plot between the fluorescence intensity ratio and the H_2O_2 concentration. Each error bar shows the standard deviation of three independent measurements. Plots of (c) F_{564}/F_{438} and (d) F_{564} versus H_2O_2 concentrations for four independent measurements.

absorptions were obtained. The above results demonstrated that C_3N_4−Ru possessed intrinsic peroxidase-like activity.

Furthermore, the effect of H_2O_2 and catalyst concentrations on the peroxidase-like activity of C_3N_4−Ru was investigated. As shown in Figure S5c,d, by monitoring the time-dependent absorption spectra, the reaction rate increased with increasing concentration of H_2O_2 or catalyst. Therefore, similar to natural peroxidase, C_3N_4−Ru also exhibited H_2O_2 and catalyst concentration-dependent peroxidase-like activity.

A comparison of the peroxidase-like activities of C_3N_4-based nanozymes was performed by monitoring the kinetics curves of OPDox. In a given time (i.e., 120 s), a larger absorbance at 450 nm indicated a higher catalytic activity. As shown in Figure 2a, the C_3N_4−Ru exhibited the highest catalytic activity while pure C_3N_4 possessed negligible peroxidase-like activity. Moreover, to quantitatively compare the catalytic activity of C_3N_4-based nanozymes, the relative activity of the nanozyme was defined in the Experimental Section. As shown in Figure 2b, the C_3N_4−Ru, C_3N_4−Cu, and C_3N_4−hemin exhibited 13.6-, 4.9-, and 4.3-fold higher catalytic activity than pure C_3N_4 nanosheets, demonstrating the weak peroxidase-like activity of C_3N_4 could be significantly enhanced by metal ions or hemin modification. The Ru in C_3N_4−Ru, Cu in C_3N_4−Cu, and Fe in C_3N_4−hemin could act as the catalytic active sites for peroxidase mimics.

After establishing the peroxidase-like activities of C_3N_4-based nanozymes, their optical properties were investigated. As shown in Figure 2c, UV−visible spectra suggested that C_3N_4-based nanozymes possessed similar absorption spectra with a maximum absorption at about 300 nm. Figure 2d showed that C_3N_4-based nanozymes had a broad excitation band ranging from 300 to 400 nm. A fluorescence emission peak at 438 nm can be observed upon exciting at 385 nm.

Robust Sensing of H_2O_2 and Glucose. Then, the fluorescent C_3N_4-based nanozymes with peroxidase-like activities were used for ratiometric bioassay development. C_3N_4−Ru was first used for H_2O_2 and glucose detection. As shown in Figure S6, C_3N_4−Ru nanosheets possessed a strong emission peak at 438 nm upon exciting at 385 nm. However, in the presence of H_2O_2 and OPD, the emission of C_3N_4−Ru was quenched, and a new emission signal at 564 nm emerged. The emerging emission peak at 564 nm was attributed to the oxidized OPD (i.e., OPDox), which was formed by H_2O_2 oxidation with the assistance of C_3N_4−Ru. According to previous studies, the OPDox could quench the fluorescence of C_3N_4 by the photoinduced electron transfer effect.[54] Therefore, for the current system, C_3N_4−Ru first catalyzed the oxidation of OPD to form OPDox. Subsequently, the OPDox was assembled onto the C_3N_4−Ru through hydrogen bond and $\pi-\pi$ stacking, resulting in the quenching of the fluorescence at 438 nm and the emergence of the emission signal at 564 nm.

The fluorescent peaks at 438 and 564 nm were then used for ratiometric sensing. First, the ratiometric sensing of H_2O_2 was performed. To evaluate the detection sensitivity and linear range, various concentrations of H_2O_2 were added into C_3N_4−Ru and OPD solutions. As illustrated in Figure 3a, the fluorescent intensity at 438 nm of C_3N_4−Ru gradually decreased while the intensity at 564 nm increased by increasing the H_2O_2 concentrations from 10 to 5000 μM. The ratiometric fluorescence intensity (F_{564}/F_{438}) exhibited a broad dynamic range for the H_2O_2 concentration from 10 to 1000 μM with a detection limit of 4.20 μM (Figure 3b). Overall, our ratiometric sensing method for H_2O_2 detection exhibited broader linear range and better sensitivity than most reported H_2O_2 sensors based on nanozymes (Table S1).

To demonstrate the unique advantages of the as-designed ratiometric fluorescent sensor over the conventional nanozyme sensor with single signal output, we compared their sensing performances toward H_2O_2 detection. As shown in Figure 3c,d, the response curves between F_{564}/F_{438} (or F_{564}) and H_2O_2

DOI: 10.1021/acs.analchem.9b01884
Anal. Chem. 2019, 91, 10648−10656

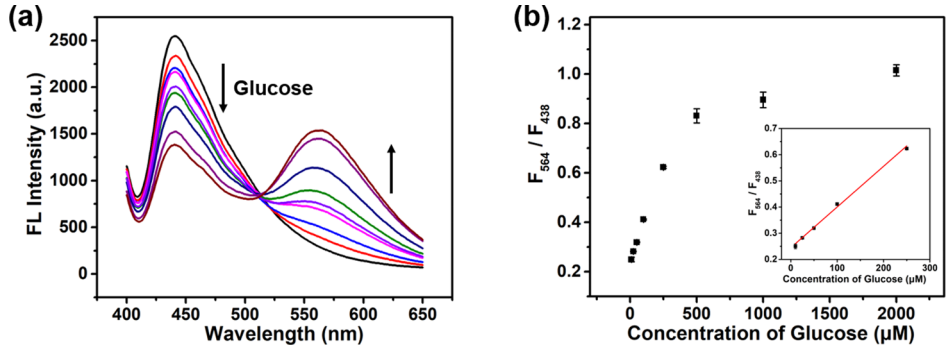

Figure 4. (a) Fluorescence spectra of C_3N_4−Ru nanozyme in the presence of 0, 10, 25, 50, 100, 250, 500, 1000, and 2000 μM of glucose. (b) Fluorescence intensity ratio (F_{564}/F_{438}) as a function of glucose concentration. Inset: linear calibration plot between the fluorescence intensity ratio and the glucose concentration. Each error bar shows the standard deviation of three independent measurements.

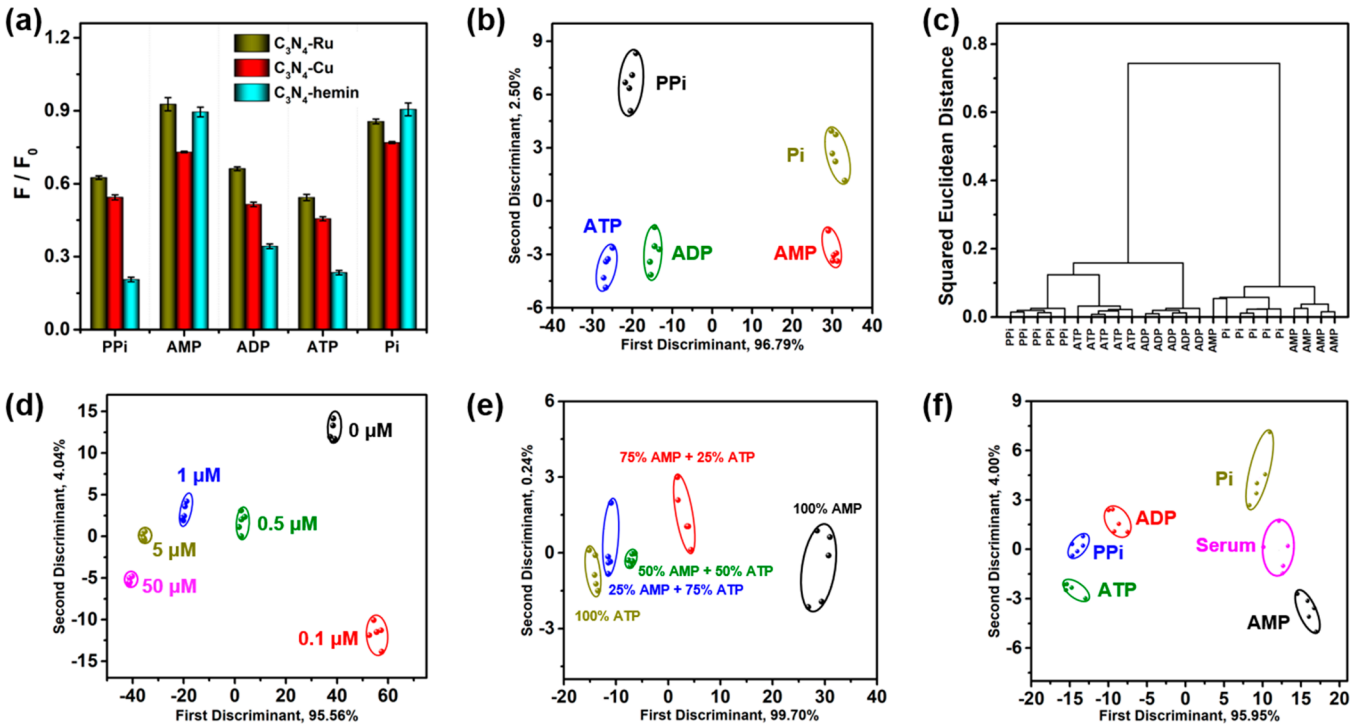

Figure 5. Ratiometric fluorescent sensor arrays for phosphates. (a) Ratiometric fluorescent response patterns (F/F_0) of sensor arrays toward 10 μM phosphates. Each error bar shows the standard deviation of five independent measurements. (b) 2D canonical score plot for the first two factors of the ratiometric fluorescent response obtained against 10 μM phosphates. (c) Hierarchical-cluster-analysis (HCA) plot for the discrimination of phosphates generated from the ratiometric fluorescence-response patterns toward 10 μM phosphates. (d−f) 2D canonical score plots for the first two factors of the ratiometric fluorescent response patterns obtained against different concentrations of ATP (d), mixture of ATP and AMP with different molar ratios and total concentrations of 2 μM (e), and 5 μM phosphates in the presence of 0.1% FBS (f). The canonical scores were calculated by LDA for the identification and discrimination of phosphates.

concentration were obtained by four independent measurements. Figure 3c shows that the obtained ratiometric signals (i.e., F_{564}/F_{438}) for four measurements were almost the same. However, when the nonratiometric sensor was applied, four measurements exhibited a large deviation, especially at low H_2O_2 concentrations (Figure 3d). The above results demonstrated that the ratiometric output signal efficiently enhanced the robustness of H_2O_2 assays.

The ratiometric sensor can be further used to detect the H_2O_2-producing metabolites (e.g., glucose, lactate, sarcosine, cholesterol, etc.). Here, we took glucose as an example to show the capability of the sensor for H_2O_2-producing metabolites. Glucose could be specifically oxidized by glucose oxidase (GOx) to generate H_2O_2. Therefore, by coupling the GOx with peroxidase-mimicking C_3N_4−Ru, glucose could be detected by the ratiometric fluorescent sensor. As shown in Figure 4a, the fluorescent peak at 438 nm was gradually quenched while the peak at 564 nm increased with increasing concentration of glucose. A calibration curve of glucose detection ranging from 10 to 2000 μM is shown in Figure 4b. Furthermore, the linear range for glucose was determined to be 10 to 250 μM with a detection limit of 4.73 μM (Figure 4b).

Ratiometric Sensor Arrays for Phosphates Discrimination. To further demonstrate the robustness of the C_3N_4-based fluorescent biosensors, ratiometric sensor arrays were constructed for phosphates detection and discrimination. Taking C_3N_4−Cu as a sample, we first studied the influences

DOI: 10.1021/acs.analchem.9b01884
Anal. Chem. 2019, 91, 10648−10656

of five phosphates on the nanozymes' catalytic activities. As shown in Figure S7a, the value of F_{564}/F_{438} decreased with the increasing of ATP concentration, demonstrating the concentration-dependent inhibitory ability of ATP on the C_3N_4-based nanozymes' catalytic activity. Furthermore, the inhibitory effects of other phosphates were also evaluated. The results presented in Figure S7b demonstrated the differential inhibitory effects of five phosphates on the peroxidase-like activity of C_3N_4−Cu. Moreover, each phosphate also possessed differential binding ability with different metal catalytic active sites (Figure S7c). The inhibitory effects of phosphates on the peroxidase-like activities of C_3N_4-based nanozymes are due to the interactions between phosphates and the catalytic active sites (i.e., Ru for C_3N_4−Ru, Cu for C_3N_4−Cu, and Fe for C_3N_4−hemin). Therefore, the sensor arrays constructed by C_3N_4−Ru, C_3N_4−Cu, and C_3N_4−hemin can give cross-reactive signals to each analyte. To evaluate the discrimination ability of the sensor arrays, the responses of nanozymes to phosphates were first evaluated. The ratiometric fluorescence response patterns (or "fingerprint maps") for 10 μM phosphates were constructed by using F/F_0, where F was the ratio of F_{564} and F_{438} in the presence of phosphates and F_0 was the ratio of F_{564} and F_{438} without phosphates. As shown in Figure 5a, the phosphates exhibited differential modulation on the catalytic oxidation of OPD with the C_3N_4-based nanozymes. Then, the response patterns were subjected to linear discriminant analysis (LDA) to generate a 2D canonical plot. As shown in Figure 5b, the canonical patterns were clustered into five groups, with all phosphates well separated from each other with no misclassification. We evaluated the advantages of ratiometric signals in phosphate discrimination by comparing with the single colorimetric output signal. The response patterns of 10 μM phosphates from the single colorimetric output signal-based sensor arrays were subjected to LDA, which produced overlapped clusters and had a narrower distance between five clusters (Figure S8). In addition to LDA, hierarchical-cluster-analysis (HCA) also showed that five phosphates could be well discriminated with no errors by the ratiometric fluorescent sensor arrays (Figure 5c). To further demonstrate the discrimination ability of the sensor arrays for phosphates, other concentrations (1 and 5 μM) of phosphates were also evaluated (Figures S9 and S10). Similar to the concentration of 10 μM, the phosphates could be efficiently differentiated with no misclassification, demonstrating the ratiometric sensor arrays exhibited excellent discrimination power for phosphates at different concentrations.

To demonstrate the quantitative ability of the ratiometric sensor array, discrimination assays for various concentrations of ATP were performed as an example. The response patterns for various concentrations of ATP were measured (Figure S11). Subsequently, LDA was used to analyze the response patterns. As shown in Figures 5d and S11, sample groups with ATP concentrations ranging from 0.1 to 50 μM were entirely separated with no misclassifications. Then, to evaluate the multiplex detection ability, we tested the discrimination capability of the sensor array toward the mixtures of ATP and AMP with different molar ratios (total concentration of 2 μM). As shown in Figures S12 and 5e, the mixtures of ATP and AMP as well as the pure ATP and AMP were clustered into different groups and all groups were clearly separated from each other, indicating that the ratiometric sensor arrays possessed excellent multiplex detection ability. Further, to demonstrate the potential applications of the as-developed sensor arrays in real samples, the discrimination of phosphates in fetal bovine serum (FBS) was investigated. As shown in Figures S13 and 5f, the sensor arrays performed well for differentiation of five phosphates at a relatively low concentration (5 μM) in 0.1% FBS.

Identifications of unknown samples were carried out to demonstrate the practical applications of the as-designed sensor arrays. The response patterns of 20 unknown samples were shown in Figure S14. On the basis of the above training matrix, the Mahalanobis squared distances between the unknown samples and the corresponding training phosphates group could be determined by LDA. The unknown samples can be identified to the corresponding phosphate group according to the minimal Mahalanobis squared distance. As shown in Table S2, 20 blind samples were identified with 95% accuracy.

CONCLUSIONS

In conclusion, we have prepared three fluorescent C_3N_4-based nanozymes with excellent peroxidase-like activities. On the basis of C_3N_4−Ru nanozymes, we first constructed a ratiometric fluorescence sensor for H_2O_2 and its related metabolite (i.e., glucose). Ratiometric fluorescent sensor arrays were then successfully constructed on the basis of C_3N_4−Ru, C_3N_4−Cu, and C_3N_4−hemin. Five phosphates were well discriminated and detected using the as-prepared ratiometric fluorescent sensor array. Encouragingly, both the ratiometric fluorescence sensors and ratiometric fluorescent sensor arrays exhibited better robustness compared with the corresponding single output signal-based ones. Furthermore, the usefulness of the ratiometric arrays was demonstrated by detecting unknown blind samples, where 20 unknown samples containing phosphates were identified with 95% accuracy. Overall, this study demonstrates a new method for constructing ratiometric nanozyme biosensing systems.

ASSOCIATED CONTENT

Supporting Information

The Supporting Information is available free of charge on the ACS Publications website at DOI: 10.1021/acs.analchem.9b01884.

TEM images, PXRD patterns, FT-IR, XPS, absorption, and fluorescence spectra, kinetic curves, colorimetric response patterns, 2D canonical score plots, ratiometric fluorescence-response patterns, comparison of the current sensing system with reported methods for H_2O_2 detection, and identification of 20 blind samples (PDF)

AUTHOR INFORMATION

Corresponding Author

*E-mail: weihui@nju.edu.cn. Fax: +86-25-83594648. Tel: +86-25-83593272.

ORCID

Xiaoyu Wang: 0000-0002-8641-2430
Hang Xing: 0000-0003-3917-8343
Hui Wei: 0000-0003-0870-7142

Author Contributions

The manuscript was written through contributions of all authors.

DOI: 10.1021/acs.analchem.9b01884
Anal. Chem. 2019, 91, 10648−10656

Notes

The authors declare no competing financial interest.

■ ACKNOWLEDGMENTS

This work was supported by National Natural Science Foundation of China (21722503, 21874067, and 91859112), 973 Program (2015CB659400), PAPD Program, Shuangchuang Program of Jiangsu Province, Open Funds of the State Key Laboratory of Analytical Chemistry for Life Science (SKLACLS1704), Open Funds of the State Key Laboratory of Coordination Chemistry (SKLCC1819), the China Postdoctoral Science Foundation (2019TQ0144), Open Funds of Key Laboratory of Analytical Chemistry for Biology and Medicine (Wuhan University), Ministry of Education (ACBM2019001), and Fundamental Research Funds for the Central Universities (021314380145).

■ REFERENCES

(1) Wu, J.; Wang, X.; Wang, Q.; Lou, Z.; Li, S.; Zhu, Y.; Qin, L.; Wei, H. *Chem. Soc. Rev.* **2019**, *48*, 1004−1076.
(2) Gao, L.; Zhuang, J.; Nie, L.; Zhang, J.; Zhang, Y.; Gu, N.; Wang, T.; Feng, J.; Yang, D.; Perrett, S.; Yan, X. *Nat. Nanotechnol.* **2007**, *2*, 577−583.
(3) Wang, X.; Guo, W.; Hu, Y.; Wu, J.; Wei, H. *Nanozymes: Next Wave of Artificial Enzymes*; Springer, 2016.
(4) Huang, Y.; Ren, J.; Qu, X. *Chem. Rev.* **2019**, *119*, 4357−4412.
(5) Wang, H.; Wan, K.; Shi, X. *Adv. Mater.* **2018**, 1805368.
(6) Wang, Q.; Zhang, X.; Huang, L.; Zhang, Z.; Dong, S. *Angew. Chem., Int. Ed.* **2017**, *56*, 16082−16085.
(7) Wei, H.; Wang, E. *Anal. Chem.* **2008**, *80*, 2250−2254.
(8) Duan, D.; Fan, K.; Zhang, D.; Tan, S.; Liang, M.; Liu, Y.; Zhang, J.; Zhang, P.; Liu, W.; Qiu, X.; Kobinger, G. P.; Gao, G. F.; Yan, X. *Biosens. Bioelectron.* **2015**, *74*, 134−141.
(9) Sun, H.; Zhou, Y.; Ren, J.; Qu, X. *Angew. Chem., Int. Ed.* **2018**, *57*, 9224−9237.
(10) Fan, K.; Cao, C.; Pan, Y.; Lu, D.; Yang, D.; Feng, J.; Song, L.; Liang, M.; Yan, X. *Nat. Nanotechnol.* **2012**, *7*, 459−464.
(11) Fan, K.; Xi, J.; Fan, L.; Wang, P.; Zhu, C.; Tang, Y.; Xu, X.; Liang, M.; Jiang, B.; Yan, X.; Gao, L. *Nat. Commun.* **2018**, *9*, 1440.
(12) Xu, B.; Wang, H.; Wang, W.; Gao, L.; Li, S.; Pan, X.; Wang, H.; Yang, H.; Meng, X.; Wu, Q.; Zheng, L.; Chen, S.; Shi, X.; Fan, K.; Yan, X.; Liu, H. *Angew. Chem., Int. Ed.* **2019**, *58*, 4911−4916.
(13) Huo, M.; Wang, L.; Chen, Y.; Shi, J. *Nat. Commun.* **2017**, *8*, 357.
(14) Zhang, W.; Hu, S.; Yin, J.-J.; He, W.; Lu, W.; Ma, M.; Gu, N.; Zhang, Y. *J. Am. Chem. Soc.* **2016**, *138*, 5860−5865.
(15) Zhen, W.; Liu, Y.; Lin, L.; Bai, J.; Jia, X.; Tian, H.; Jiang, X. *Angew. Chem., Int. Ed.* **2018**, *57*, 10309−10313.
(16) Zhang, Z.; Zhang, X.; Liu, B.; Liu, J. *J. Am. Chem. Soc.* **2017**, *139*, 5412−5419.
(17) Ye, H.; Yang, K.; Tao, J.; Liu, Y.; Zhang, Q.; Habibi, S.; Nie, Z.; Xia, X. *ACS Nano* **2017**, *11*, 2052−2059.
(18) Soh, M.; Kang, D.-W.; Jeong, H.-G.; Kim, D.; Kim, D. Y.; Yang, W.; Song, C.; Baik, S.; Choi, I.-Y.; Ki, S.-K.; Kwon, H. J.; Kim, T.; Kim, C. K.; Lee, S.-H.; Hyeon, T. *Angew. Chem., Int. Ed.* **2017**, *56*, 11399−11403.
(19) Chong, Y.; Dai, X.; Fang, G.; Wu, R.; Zhao, L.; Ma, X.; Tian, X.; Lee, S.; Zhang, C.; Chen, C.; Chai, Z.; Ge, C.; Zhou, R. *Nat. Commun.* **2018**, *9*, 4861.
(20) Tang, W.; Fan, W.; Zhang, W.; Yang, Z.; Li, L.; Wang, Z.; Chiang, Y.-L.; Liu, Y.; Deng, L.; He, L.; Shen, Z.; Jacobson, O.; Aronova, M. A.; Jin, A.; Xie, J.; Chen, X. *Adv. Mater.* **2019**, *31*, 1900401.
(21) Vernekar, A. A.; Sinha, D.; Srivastava, S.; Paramasivam, P. U.; D'Silva, P.; Mugesh, G. *Nat. Commun.* **2014**, *5*, 5301.
(22) Vernekar, A. A.; Das, T.; Mugesh, G. *Angew. Chem., Int. Ed.* **2016**, *55*, 1412−1416.
(23) Natalio, F.; Andre, R.; Hartog, A. F.; Stoll, B.; Jochum, K. P.; Wever, R.; Tremel, W. *Nat. Nanotechnol.* **2012**, *7*, 530−535.
(24) Herget, K.; Hubach, P.; Pusch, S.; Deglmann, P.; Goetz, H.; Gorelik, T. E.; Gural'skiy, I. y. A.; Pfitzner, F.; Link, T.; Schenk, S.; Panthoefer, M.; Ksenofontov, V.; Kolb, U.; Opatz, T.; Andre, R.; Tremel, W. *Adv. Mater.* **2017**, *29*, 1603823.
(25) Kim, M. I.; Park, K. S.; Park, H. G. *Chem. Commun.* **2014**, *50*, 9577−9580.
(26) Song, Y.; Wang, Y.; Qin, L. *J. Am. Chem. Soc.* **2013**, *135*, 16785−16788.
(27) Deng, H.-H.; Luo, B.-Y.; He, S.-B.; Chen, R.-T.; Lin, Z.; Peng, H.-P.; Xia, X.-H.; Chen, W. *Anal. Chem.* **2019**, *91*, 4039−4046.
(28) Zhang, X.; Liu, W.; Li, X.; Zhang, Z.; Shan, D.; Xia, H.; Zhang, S.; Lu, X. *Anal. Chem.* **2018**, *90*, 14309−14315.
(29) Gao, Z.; Liu, G. G.; Ye, H.; Rauschendorfer, R.; Tang, D.; Xia, X. *Anal. Chem.* **2017**, *89*, 3622−3629.
(30) Wang, X.; Hu, Y.; Wei, H. *Inorg. Chem. Front.* **2016**, *3*, 41−60.
(31) Liu, B.; Huang, Z.; Liu, J. *Nanoscale* **2016**, *8*, 13562−13567.
(32) Hu, Y.; Cheng, H.; Zhao, X.; Wu, J.; Muhammad, F.; Lin, S.; He, J.; Zhou, L.; Zhang, C.; Deng, Y.; Wang, P.; Zhou, Z.; Nie, S.; Wei, H. *ACS Nano* **2017**, *11*, 5558−5566.
(33) Han, L.; Zhang, H.; Chen, D.; Li, F. *Adv. Funct. Mater.* **2018**, *28*, 1800018.
(34) Wang, X.; Cao, W.; Qin, L.; Lin, T.; Chen, W.; Lin, S.; Yao, J.; Zhao, X.; Zhou, M.; Hang, C.; Wei, H. *Theranostics* **2017**, *7*, 2277−2286.
(35) Kim, M. S.; Cho, S.; Joo, S. H.; Lee, J.; Kwak, S. K.; Kim, M. I.; Lee, J. *ACS Nano* **2019**, *13*, 4312−4321.
(36) Huang, Y.; Zhao, M.; Han, S.; Lai, Z.; Yang, J.; Tan, C.; Ma, Q.; Lu, Q.; Chen, J.; Zhang, X.; Zhang, Z.; Li, B.; Chen, B.; Zong, Y.; Zhang, H. *Adv. Mater.* **2017**, *29*, 1700102.
(37) Cheng, H.; Zhang, L.; He, J.; Guo, W.; Zhou, Z.; Zhang, X.; Nie, S.; Wei, H. *Anal. Chem.* **2016**, *88*, 5489−5497.
(38) Fang, X.; Zheng, Y.; Duan, Y.; Liu, Y.; Zhong, W. *Anal. Chem.* **2019**, *91*, 482−504.
(39) Qiu, H.; Pu, F.; Ran, X.; Liu, C.; Ren, J.; Qu, X. *Anal. Chem.* **2018**, *90*, 11775−11779.
(40) Wang, Y.-M.; Liu, J.-W.; Adkins, G. B.; Shen, W.; Trinh, M. P.; Duan, L.-Y.; Jiang, J.-H.; Zhong, W. *Anal. Chem.* **2017**, *89*, 12327−12333.
(41) Weerathunge, P.; Ramanathan, R.; Torok, V. A.; Hodgson, K.; Xu, Y.; Goodacre, R.; Behera, B. K.; Bansal, V. *Anal. Chem.* **2019**, *91*, 3270−3276.
(42) Wei, X.; Chen, Z.; Tan, L.; Lou, T.; Zhao, Y. *Anal. Chem.* **2017**, *89*, 556−559.
(43) Boriachek, K.; Masud, M. K.; Palma, C.; Phan, H.-P.; Yamauchi, Y.; Hossain, M. S. A.; Nguyen, N.-T.; Salomon, C.; Shiddiky, M. J. A. *Anal. Chem.* **2019**, *91*, 3827−3834.
(44) Gao, L.; Liu, M.; Ma, G.; Wang, Y.; Zhao, L.; Yuan, Q.; Gao, F.; Liu, R.; Zhai, J.; Chai, Z.; Zhao, Y.; Gao, X. *ACS Nano* **2015**, *9*, 10979−10990.
(45) Wang, X.; Qin, L.; Zhou, M.; Lou, Z.; Wei, H. *Anal. Chem.* **2018**, *90*, 11696−11702.
(46) Qin, L.; Wang, X.; Liu, Y.; Wei, H. *Anal. Chem.* **2018**, *90*, 9983−9989.
(47) Li, X.; Wen, F.; Creran, B.; Jeong, Y.; Zhang, X.; Rotello, V. M. *Small* **2012**, *8*, 3589−3592.
(48) Rana, S.; Elci, S. G.; Mout, R.; Singla, A. K.; Yazdani, M.; Bender, M.; Bajaj, A.; Saha, K.; Bunz, U. H. F.; Jirik, F. R.; Rotello, V. M. *J. Am. Chem. Soc.* **2016**, *138*, 4522−4529.
(49) Lee, M. H.; Kim, J. S.; Sessler, J. L. *Chem. Soc. Rev.* **2015**, *44*, 4185−4191.
(50) Pode, Z.; Peri-Naor, R.; Georgeson, J. M.; Ilani, T.; Kiss, V.; Unger, T.; Markus, B.; Barr, H. M.; Motiei, L.; Margulies, D. *Nat. Nanotechnol.* **2017**, *12*, 1161−1168.
(51) Sun, S.; Jiang, K.; Qian, S.; Wang, Y.; Lin, H. *Anal. Chem.* **2017**, *89*, 5542−5548.
(52) Zhou, Z.; Zhang, Y.; Shen, Y.; Liu, S.; Zhang, Y. *Chem. Soc. Rev.* **2018**, *47*, 2298−2321.

DOI: 10.1021/acs.analchem.9b01884
Anal. Chem. 2019, 91, 10648−10656

(53) Ong, W.-J.; Tan, L.-L.; Ng, Y. H.; Yong, S.-T.; Chai, S.-P. *Chem. Rev.* **2016**, *116*, 7159−7329.
(54) Liu, J.-W.; Luo, Y.; Wang, Y.-M.; Duan, L.-Y.; Jiang, J.-H.; Yu, R.-Q. *ACS Appl. Mater. Interfaces* **2016**, *8*, 33439−33445.
(55) Lin, T.; Zhong, L.; Wang, J.; Guo, L.; Wu, H.; Guo, Q.; Fu, F.; Chen, G. *Biosens. Bioelectron.* **2014**, *59*, 89−93.
(56) Hargrove, A. E.; Nieto, S.; Zhang, T.; Sessler, J. L.; Anslyn, E. V. *Chem. Rev.* **2011**, *111*, 6603−6782.
(57) Ju, E.; Dong, K.; Chen, Z.; Liu, Z.; Liu, C.; Huang, Y.; Wang, Z.; Pu, F.; Ren, J.; Qu, X. *Angew. Chem., Int. Ed.* **2016**, *55*, 11467−11471.
(58) Peng, Y.; Lu, B.; Chen, L.; Wang, N.; Lu, J. E.; Ping, Y.; Chen, S. *J. Mater. Chem. A* **2017**, *5*, 18261−18269.
(59) Creutz, C.; Sutin, N. *Proc. Natl. Acad. Sci. U. S. A.* **1975**, *72*, 2858−2862.
(60) Agnes, C.; Arnault, J.-C.; Omnes, F.; Jousselme, B.; Billon, M.; Bidan, G.; Mailley, P. *Phys. Chem. Chem. Phys.* **2009**, *11*, 11647−11654.

DOI: 10.1021/acs.analchem.9b01884
Anal. Chem. 2019, 91, 10648−10656